

## Low energy quasiparticle dispersion of graphite by angle-resolved photoemission spectroscopy

A. Grüneis<sup>\*1</sup>, T. Pichler<sup>1</sup>, H. Shiozawa<sup>1</sup>, C. Attaccalite<sup>2</sup>, L. Wirtz<sup>2</sup>, S. L. Molodtsov<sup>3</sup>, R. Follath<sup>4</sup>, R. Weber<sup>4</sup>, and A. Rubio<sup>5</sup>

<sup>1</sup> IFW Dresden, P.O. Box 270116, 01171 Dresden, Germany

<sup>2</sup> Institute for Electronics, Microelectronics, and Nanotechnology Dept. ISEN, B.P. 60069, 59652 Villeneuve d'Ascq Cedex, France

<sup>3</sup> Institut für Festkörperphysik, TU Dresden, Mommsenstrasse 13, 01069 Dresden, Germany

<sup>4</sup> BESSY II, Albert-Einstein-Str. 15, 12489 Berlin, Germany

<sup>5</sup> Dept. Fisica de Materiales, Donostia International Physics Center, European Theoretical Spectroscopy Facility (ETSF), Spain

Received 8 June 2007, accepted 18 June 2007

Published online 25 October 2007

PACS 61.46.Fg, 73.21.–b, 79.60.Bm

The low energy electron dispersion in graphite is measured by angle-resolved photoemission spectroscopy. The measured photoemission intensity maxima are compared to a tight-binding calculation of the electronic band structure. We observe a strong trigonal warping of the equi-energy contour which is well reproduced by the calculations. Furthermore we clearly show that the concept of Dirac Fermions breaks down for AB stacked graphite.

© 2007 WILEY-VCH Verlag GmbH & Co. KGaA, Weinheim

### 1 Introduction

Graphite is the simplest layered material and has been extensively studied over the past 60 years [1, 2]. Its electronic properties are very sensitive to stacking and the number of layers [3]. Two-dimensional graphene is a zero-gap semiconductor and three-dimensional (3D) graphite (AB stacking) is a semimetal. Recently, angle resolved photoemission spectroscopy (ARPES) has shown that electron–phonon [4] and electron–plasmon [5] interactions are responsible for kinks in the quasiparticle dispersions and lifetimes of graphene and graphite. Furthermore it was claimed from ARPES that the low energy excitations at the Brillouin zone (BZ) boundaries are Dirac Fermions, i.e. a linear electronic dispersion relation around the Fermi level ( $E_F$ ) [6]. Few layered graphene also has a potential application as a nanoelectronic device. Recently it was used to successfully fabricate a semimetal field effect transistor [7]. A gap that is tunable with gate voltage was observed by ARPES in a graphite bilayer [8].

As a result of the small dispersion of the electronic bands in the direction perpendicular to the layers ( $k_z$ ) and the fact that single-crystals of graphite are rare, the 3D nature of graphite has often been neglected. For electronic structure calculations of graphite, the local-density approximation (LDA) is often used. However, it was shown by ARPES [9] that the LDA strongly underestimates the slope of the electronic bands and a scaling has to be applied. The precise slope of the electronic bands is important for determination of the optical and transport and related condensed-matter properties. The slope of the quasiparticle dispersion and the strength of the trigonal warping effect are also important for the double resonant Raman process [10–12]. The electronic bands calculated by the so-called GW approximation

\* Corresponding author: e-mail: ag3@biela.ifw-dresden.de, Phone: +49 351 4659 713, Fax: +49 351 4659 440

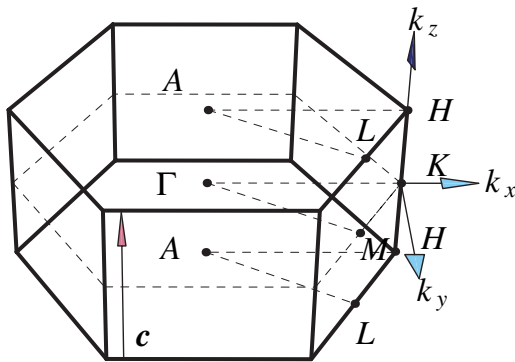


**Fig. 1** (online colour at: [www.pss-b.com](http://www.pss-b.com)) First Brillouin zone of graphite with the high symmetry points  $\Gamma$ , K and M in the  $k_z = 0$  plane. A, H and L are in the  $k_z = 0.47 \text{ \AA}^{-1}$  plane. The reciprocal lattice vector perpendicular to the graphene layers is  $c$ .

were found to be in much better agreement to the experiment than ARPES [9]. This indicates that electronic correlation effects play a crucial role for the renormalization of the electronic band structure. Apart from LDA and GW, there is also a set of tight-binding parameters which was fit to transport and optical spectroscopy experiments [13]. In this contribution we calculate the electronic structure around the Fermi level by tight-binding and compare the calculated results to the measured photoemission intensity maxima.

## 2 Tight-binding description of graphite

The graphite unitcell has four atoms and each atom contributes one electron to make up the  $\pi$  electronic bands. TB calculations for the  $\pi$  bands are carried out with the Slonczewski–Weiss–McClure (SWMC) Hamiltonian [2]. This Hamiltonian depends on eight parameters that were previously fitted to various optical and transport experiments [13]. The TB parameters are directly related to the band structure, e.g.  $\gamma_0$  to  $\gamma_5$  are the transfer integrals affecting the Fermi velocity ( $v_F$ ), trigonal warping, energy separation of valence bands and  $\Delta$ , which is the difference in the on-site potentials is related to a pseudogap at the H-point [14]. The last parameter,  $E_F$ , determines the Fermi level. In Fig. 1 the first Brillouin zone (BZ) of graphite is shown. The calculated band structure in the  $k_x$ – $k_y$  plane for constant  $k_z$  is shown in Fig. 2 in (a) for K and in (b) for H-point. It is clear that around K four bands can be seen while around H only two non-degenerate bands appear. Furthermore the dispersion is parabolic at K while it is close to linear at H. As such the bands in H have been interpreted as Dirac Fermion like. However it is long known that graphite in an AB stacking order has a small gap at H which is related to a crystal field effect since the

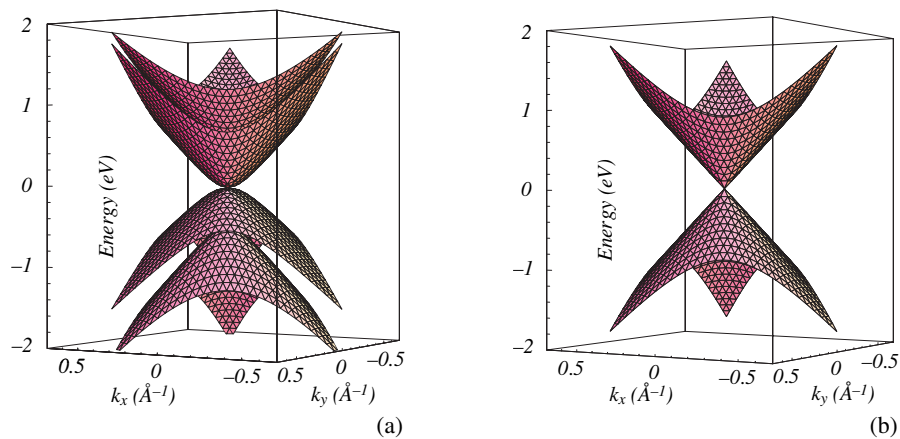


**Fig. 2** (online colour at: [www.pss-b.com](http://www.pss-b.com)) Calculated tight-binding band structure in the  $k_x$ – $k_y$ -plane is shown in (a) for K and in (b) for H.

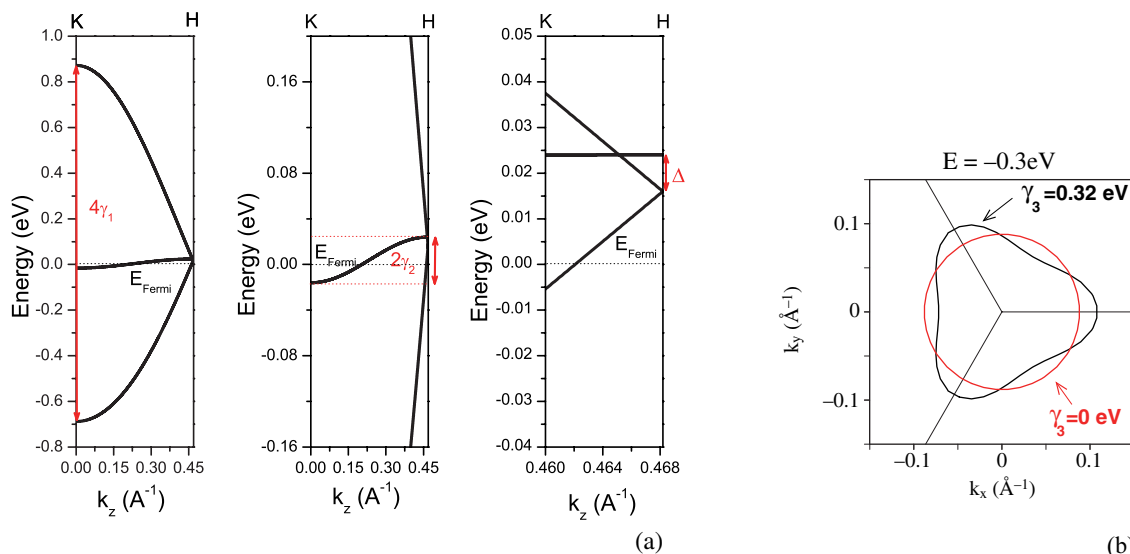


**Fig. 3** (online colour at: [www.pss-b.com](http://www.pss-b.com)) (a) Dispersion calculated by TB from K to H. In this calculation we fixed  $k_x = k_y = 0$ . The matrix elements  $\gamma_1$  and  $\gamma_2$  that determine the bandwidths in  $k_z$  direction are shown. The pseudogap  $\Delta$  which causes a breakdown of Dirac Fermions in graphite is also shown. (b) Equi-energy contour for 0.3 eV binding energy. The strength of the trigonal warping effect is determined by  $\gamma_3$ . Here the same equi-energy contour for a finite (black line) and a zero value (red line) of  $\gamma_3$  are shown.

potential for A and B atoms is not equal to each other. This gap is described by the TB parameter  $\Delta$  and appears in the diagonal elements of the Hamiltonian. Experimentally there is only one work that reports  $\Delta = 8$  meV [14]. The finite value of  $\Delta$  induces a high curvature for the  $\pi$  bands at H and results in a breakdown of the linear dispersion. In Fig. 3(a) the dispersion in  $k_z$  direction is shown and the bandwidth is shown in terms of the TB matrix elements  $\gamma_1$  and  $\gamma_2$ . The splitting between the two valence bands is a maximum at K and the bands become degenerate at H. The pseudogap  $\Delta$  is shown in the right panel of Fig. 3(a). In Fig. 3(b) we investigate the trigonal warping effect which is determined by  $\gamma_3$ . For  $\gamma_3 = 0$  the equi-energy contours become circles around the KH-axis while a finite value of  $\gamma_3$  distorts these circles to a triangular shape, i.e. a trigonal warping effect.

### 3 Experiments and setup

Experiments were done at BESSY II using the U125/1-PGM beamline and a Scienta SES 100 analyzer with photon energies in the range of 25–100 eV. An energy resolution of 15 meV and a momentum resolution better than  $0.01 \text{ \AA}^{-1}$  was achieved. Pure natural graphite single crystals with AB stacking were cleaved in-situ to give mirror-like surfaces and were measured within 12 h after cleavage in a vacuum better than  $10^{-10}$  mbar. The samples were mounted on a three axis manipulator that could be cooled down by liquid He to 25 K. The binding energies are evaluated from experiments by taking the angle-integrated ARPES spectrum and fitting it with a Fermi function. The three-step model [15] for ARPES is employed for analysis of the  $k_z$  dispersion. After a dipole transition to an intermediate state in an inner potential  $V_0$ , the electron travels to the surface and is then scattered into a free electron parabola outside the crystal, reducing only  $k_z$ , while the wavevector parallel to the surface  $\mathbf{k}_\parallel = (k_x, k_y)$  is conserved.  $V_0$  was determined using the fact that at  $k_z = 0$  (K-point) the energy separation between the two  $\pi$  valence bands has a maximum because of symmetry. This method yields  $V_0 = 16.4 \pm 0.1$  eV which is in the same range of values determined previously [4, 16]. Hereafter any  $k_z$ -plane could be set by changing the photon energy and the polar angle [15] and polar maps at selected  $k_z$  in the  $k_x, k_y$ -plane were measured.

## 4 Results and discussion

Using the procedure and the inner potential as described above, we find that for a photon energy of 25 eV we get a  $k_z = 0.22 \text{ \AA}^{-1}$ . A comparison of the measured data to theory is then straightforward since we know the electron wavevector  $\mathbf{k}$  from experiment. The SWMC Hamiltonian  $H(\mathbf{k})$  is diagonalized by solving  $H(\mathbf{k}) \mathbf{c}(\mathbf{k}) = E(\mathbf{k}) \mathbf{c}(\mathbf{k})$ . The tight binding matrix elements we use are given in [13]. We plot the experimental and calculated electron energy dispersion relations for  $k_z = 0.22 \text{ \AA}^{-1}$  as a function of  $k_x$  and  $k_y$  in Fig. 4. For accurate determination of the quasiparticle band position we take the electron dispersion curve (EDC) maxima. It can be seen that there is a trigonal warping effect in the EDC maxima that agrees almost perfectly with the calculated equi-energy contour. Comparing to a monolayer of graphene, we find that trigonal warping in graphite is higher by a factor of  $\sim 1.5$  when considering the distances in the two high-symmetry directions. A strong asymmetry around the KH-axis in the photoemission intensity is also observed. This can be seen in Fig. 4 and is attributed to the dipole matrix element for the transition from a valence band state to an unoccupied state 25 eV above  $E_F$  [17]. From a detail analysis of the whole three-dimensional band structure we extract the following quantities. The Fermi velocity is equal to  $1.06 \times 10^6 \text{ m/s}$ . For the average in-plane electron and hole masses, we obtain  $m_e^* = 0.10m_0$  and  $m_h^* = -0.04m_0$ , respectively that is in good agreement with a previous magnetorefectance study ( $m_0$  is the free electron mass) [18]. For the out-of-plane electron and hole masses,  $m_{ze}^*$  and  $m_{zh}^*$ , we obtain  $m_{ze}^* = 22m_0$  and  $m_{zh}^* = -22m_0$ . From Fig. 3(a) it is clear that there is a weakly dispersing band crossing the Fermi level. The bandwidth of this band is equal to  $2\gamma_2$ , where  $\gamma_2$  is the transfer integral of atoms in next nearest neighbour planes. This small interaction is responsible for the large effective masses in the direction perpendicular to the graphene layers. This huge ratio of about 200 for the effective masses in the out-of-plane and in the in-plane direction is for a great part responsible for the anisotropy in the electrical conductivity and in the plasmon frequencies. From a simple Drude model for the DC electrical conductivity  $\sigma$ , we have  $\sigma = n_e e^2 \tau / m_e^* + n_h e^2 \tau / m_h^*$ , where  $n_e$  and  $n_h$  are the electron and hole concentrations, respectively and  $\tau$  the scattering time. For the in-plane (out-of-plane) conductivity, we have the effective masses in-plane (out-of-plane) as determined before. This yields a ratio of  $\sim 200$  for the conductivities, assuming that the scattering times in the in-plane and out-of-plane directions are equal to each other. A similar argument holds for the plasmon frequencies for in-plane and out-of-plane directions. A free carrier plasmon energy in a 3D material is given by  $\hbar\omega = \hbar\sqrt{n_e e^2 / (m_e^* \epsilon_0 \epsilon)}$ , where  $\epsilon$  is the dielectric screening. Here the in-plane and out-of-plane plasmon oscillations are obtained by putting the in-plane and out-of-plane effective masses and the dielectric constants in in-plane and out-of-plane direction, respectively. Using  $\epsilon_a = 5.4$  [19] and  $\epsilon_c = 1.25$  [20] for the in-plane and out-of-plane dielectric constants, respectively yields a ratio of  $\sim 7$  for the plasmon energies for in-plane and out-of-plane vibrations.

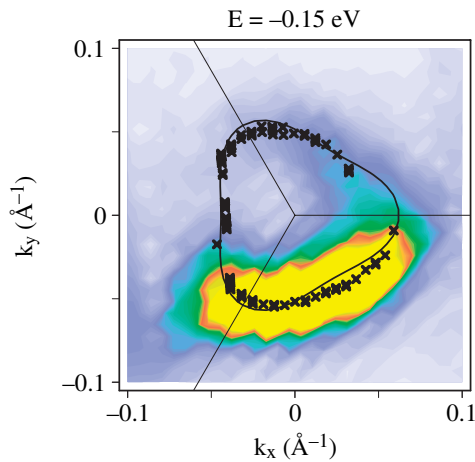


**Fig. 4** (online colour at: [www.pss-b.com](http://www.pss-b.com)) Colour code denotes the measured photoemission intensities with a photon energy of 25 eV. The crosses are the experimentally determined maxima of the EDCs (see text). This plot corresponds to a binding energy of 150 meV. The black line denotes the tight-binding calculation.

## 5 Conclusion

In conclusion we have calculated the graphite band structure by the TB approximation and compared to the experimental ARPES spectra at low binding energy. The trigonal warping effect in the EDC maxima is well reproduced by the calculation. From TB calculation we conclude that there is no Dirac Fermion at H-point in graphite. Values for the Fermi velocity and the effective masses were given and the anisotropy of the electrical conductivity and the plasmon frequencies was discussed in terms of the effective masses.

**Acknowledgements** A.G. acknowledges a Marie Curie Individual Fellowship from the European Union. C.A. and L.W. acknowledge support from the French national research agency. A.R. is supported by the EC Network of Excellence Nanoquanta (NMP4-CT-2004-500198), SANES project (NMP4-CT-2006-017310), Basque Country University (SGIker Arina), MCyT.

## References

- [1] P. R. Wallace, *Phys. Rev.* **71**, 622 (1947).
- [2] R. C. Tatar and S. Rabi, *Phys. Rev. B* **25**, 4126 (1982).
- [3] S. Latil and L. Henrard, *Phys. Rev. Lett.* **97**, 36803 (2006).
- [4] S. Y. Zhou, G. H. Gweon, and A. Lanzara, *Ann. Phys.* **321**, 1730 (2006).
- [5] A. Bostwick, T. Ohta, T. Seyller, K. Horn, and E. Rotenberg, *cond-mat/0609660* (2006).
- [6] S. Y. Zhou, G. H. Gweon, J. Graf, A. V. Fedorov, C. D. Spataru, R. D. Diehl, Y. Kopelevich, D. H. Lee, S. G. Louie, and A. Lanzara, *Nature Phys.* **69**, 245419 (2006).
- [7] K. S. Novoselov, A. K. Geim, S. V. Morozov, D. Jiang, Y. Zhang, S. V. Dubonos, I. V. Grigorieva, and A. A. Firsov, *Science* **306**, 666 (2006).
- [8] T. Ohta, A. Bostwick, T. Seyller, K. Horn, and E. Rotenberg, *Science* **313**, 951 (2006).
- [9] A. Grüneis, C. Attaccalite, T. Pichler, V. Zabolotnyy, H. Shiozawa, S. L. Molodtsov, D. Inosov, A. Koitzsch, M. Knupfer, J. Schiessling, R. Follath, R. Weber, P. Rudolf, L. Wirtz, and A. Rubio, submitted to *Phys. Rev. Lett.*, available at *cond-mat/0704.2682* (2007).
- [10] C. Thomsen and S. Reich, *Phys. Rev. Lett.* **85**, 5214 (2000).
- [11] R. Saito, A. Jorio, A. G. Souza Filho, A. Grüneis, M. A. Pimenta, G. Dresselhaus, and M. S. Dresselhaus, *Physica B* **323**, 100 (2002) (Carbon Nanotubes: Tenth Anniversary Symposium Proceedings, Tsukuba, October 2001).
- [12] A. Grüneis, R. Saito, T. Kimura, L. G. Cançado, M. A. Pimenta, A. Jorio, A. G. Souza Filho, G. Dresselhaus, and M. S. Dresselhaus, *Phys. Rev. B* **65**, 155405 (2002).
- [13] M. S. Dresselhaus and G. Dresselhaus, *Adv. Phys.* **30**, 139 (1981).
- [14] W. W. Toy, M. S. Dresselhaus, and G. Dresselhaus, *Phys. Rev. B* **15**, 4077 (1977).
- [15] S. Hüfner, *Photoelectron Spectroscopy* (Springer-Verlag, Berlin, 1996).
- [16] A. R. Law, M. T. Johnson, and H. P. Hughes, *Phys. Rev. B* **34**, 4289 (1986).
- [17] E. L. Shirley, L. J. Terminello, A. Santoni, and F. J. Himpsel, *Phys. Rev. B* **51** (1995).
- [18] E. Mendez, T. C. Chieu, N. Kambe, and M. S. Dresselhaus, *Solid State Commun.* **33**, 837 (1980).
- [19] H. Venghaus, *phys. stat. sol. (b)* **71**, 609 (1975).
- [20] E. T. Jensen, R. E. Palmer, and W. Allison, *Phys. Rev. Lett.* **66**, 492 (1991).